DNS OF A MACH 4 REACTING TURBULENT BOUNDARY LAYER

M.P. MARTIN AND G.V. CANDLER
University of Minnesota
Department of Aerospace Engineering and Mechanics
Army High Performance Computing Research Center
110 Union St. SE, Minneapolis, MN 55455

Abstract. A direct numerical simulation approach is used to study a Mach 4, $Re_\theta = 8200$ turbulent boundary layer. The conditions chosen represent a 26° wedge at a Mach number of 20 and 20 km altitude. In this case, the boundary layer temperature is high enough to induce chemical reactions. It is found that endothermic reactions result in a reduction in the magnitude of the temperature fluctuations. However, when the reactions are exothermic, the temperature and the reaction rate fluctuations are enhanced.

1. Introduction

The boundary layers on proposed air-breathing hypersonic cruise vehicles will be hot, turbulent and chemically reacting. To design these hypersonic vehicles, we need a clear understanding of the physical processes that govern these flows. For this reason, we perform direct numerical simulations (DNS) of hypersonic reacting turbulent boundary layers.

Thus far, our understanding of the interaction between turbulent motion and chemical reactions in hypersonic flows is somewhat limited. With the very high energies present in hypersonic flows, the temperature fluctuations will be very large. The reaction rate depends exponentially on temperature, and temperature fluctuations result in large increases in the reaction rates. Also, the chemical source term can either damp or amplify turbulent fluctuations. Recent linear stability analysis by Johnson *et al.* (1998) has shown that hypersonic boundary layers tend to be stabilized by endothermic reactions and destabilized by exothermic reactions.

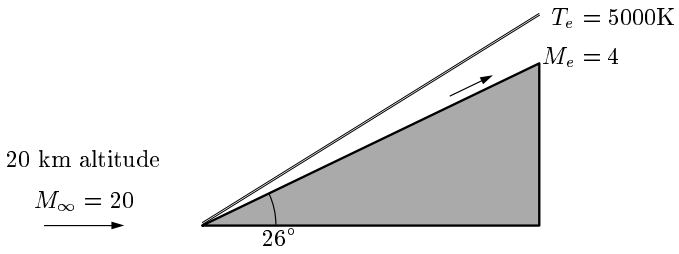

Figure 1. Flow conditions for the direct numerical simulations of boundary layers.

Martín and Candler (1998) use DNS to perform a fundamental study of isotropic turbulence interacting with finite-rate chemical reactions at conditions typical of a hypersonic boundary layer. They find that the turbulent motion is fed from the energy provided by the exothermic reactions, while the reaction rate is increased by the turbulent temperature fluctuations. This is a feedback process that takes place through the pressure-strain term in the Reynolds stress equation. The feedback is negative for endothermic reactions, resulting in a reduction in the turbulent motion.

To generalize the findings from the isotropic simulations, DNS of turbulent reacting boundary layers are presented. The conditions chosen are $Re_\theta = 8200$, $M_\infty = 4.0$, $T_\infty = 5000$ K, and $\rho_\infty = 0.5$ kg/m^3. These conditions represent a 26° wedge at a Mach number of 20 and 20 km altitude and are illustrated in Fig. 1. In this case, the boundary layer temperature is high enough to induce chemical reactions. We use a single model reaction, S1 + M $\rightleftharpoons$ S2 + M, where species S1 and S2 have the same molecular weight, that of diatomic nitrogen, M_{N_2}. The dissociation reaction rate corresponds to a nitrogen dissociation reaction.

The remainder of the paper is organized as follows. We first discuss the numerical method and initial condition for the simulations. We describe results for the non-reacting turbulent boundary layer. Finally, we compare the non-reacting, endothermic, and exothermic simulation results.

2. Numerical method and initial conditions

The numerical method combines an ENO scheme for the inviscid fluxes with an implicit time advancement technique. The ENO scheme was designed for low dissipation by Weirs *et al.* (1997) and provides shock-capturing, which is necessary at the Mach numbers considered. The time advancement technique is based on the DPLU relaxation method of Candler *et al.* (1994) and was extended to second-order accuracy by Olejniczak and Candler (1997). The derivatives required for the viscous terms are evaluated using 4th-order central differences.

The implementation of the numerical scheme has been successfully validated in Martín *et al.* (1998) by performing a DNS of a non-reacting turbulent boundary layer at $Re_\theta = 740$, $M = 0.3$, $T_\mathrm{w} = T_\infty = 300$ K, and $\rho_\infty = 1$ kg/m^3, and by comparing the results to experimental data.

The initial conditions chosen for the supersonic boundary layer simulations are $Re_\theta = 7000$, $M_\infty = 4.0$, $T_\infty = 5000$ K, and $\rho_\infty = 0.5$ kg/m^3. The size of the domain in both homogeneous directions needs to be long enough to enclose a good statistical sample of the large structures. It is found that the lengths of 4δ, and 2δ in the streamwise and spanwise directions, respectively, are adequate. In the wall-normal direction, the length of the domain is determined so that acoustic disturbances originating in the upper boundary do not interact with the boundary layer on the lower wall. The x, y, and z coordinates correspond to the streamwise, spanwise, and wall-normal directions, respectively. The number of grid points is $192 \times 128 \times 128$. The resolution for this grid is $15\Delta x^+ \times 11\Delta y^+$ in the homogenous directions. The grid is stretched in the wall-normal direction and the grid-stretching factor is 1.069. The first point away from the wall is located at $z^+ = 0.13$, and there are 28 grid points below $z^+ = 10$.

The boundary condition in the streamwise direction is periodic. Thus, the outflow conditions are used as in flow conditions and the boundary layer is allow to grow in time as the simulation progresses. Low speed simulations with these type of boundary conditions are jeopardized, since the amount of kinetic energy at the boundary layer edge may not be sufficient to maintain the turbulence levels in the boundary layer. However, this is not an issue in the present simulations, since the kinetic energy at the boundary layer edge is substantial. The boundary condition in the spanwise direction is periodic, and the boundary condition at the boundary layer edge is supersonic.

The initialization of compressible turbulence is the art of making an educated guess. In the following simulations, the mean velocity, density, and temperature turbulent profiles, and the inner parameters, u_τ and z_τ, at desired Mach number are obtained from a $k-\epsilon$ Reynolds-averaged Navier-Stokes simulation (Jones and Launder, 1992). The fluctuating velocity fields are obtained by normalizing the Mach 0.3 velocity fluctuations (Martín *et al.*, 1998) by the ratio of the inner parameters at the high Mach number to that at M =0.3. In this way, the initial fluctuating fields are scaled in proportion to the Mach number, and the initial turbulence structures and energy spectra resemble those of a realistic turbulent boundary layer. The initial fluctuations in the thermodynamic variables are estimated using the strong Reynolds analogy (Morkovin, 1962).

The chemical reactions are turned on after the boundary layer simulation reaches a stationary state based on a constant distribution of the turbulent kinetic energy scaled on inner variables. The binary reaction

$S1 + M \rightleftharpoons S2 + M$ is used, and both species have the same molecular weight, M_{N_2}, and internal degrees of freedom, so that the gas constant and specific heat do not change during the simulation. The species mass fractions are initialized to their equilibrium values at the mean temperature and density. Although the chemical composition in typical hypersonic boundary layers is not in equilibrium, this initialization serves to isolate the effect of turbulent fluctuations in the turbulence-chemistry interaction. For the conditions chosen, the reaction is endothermic. To achieve exothermicity for the purpose of comparison, we change the sign of the heat of formation.

3. Non-reacting simulations

After initializing the flow, the turbulent kinetic energy is found to be out of equilibrium. The non-reacting adiabatic boundary layer simulation reaches a stationary state near $t/\tau_\Lambda = 12$, where t is the time and $\tau_\Lambda = \delta/U_\infty$. The Reynolds number increases during the simulation, the results are shown for $t/\tau_\Lambda = 12$, and $Re_\theta = 8200$.

Figure 2 plots the two-point correlations, showing that the turbulent structures are not correlated in the middle of the box. Thus, the size of the box remains large enough to perform a DNS at the conditions chosen. Figure 3 plots the energy spectra for various quantities in the logarithmic region, $z^+ = 110$, and in the viscous sublayer, $z^+ = 4.25$. The Reynolds number for the simulation is large enough so that the energy spectra develop an inertial range. Furthermore, there are about 4 decades of decay, showing that the turbulence is well resolved.

Figure 4 plots the mean velocity profile scaled on the inner variables. The data agree with the theoretical values in the viscous region. However, the data fail to match the empirical law in the logarithmic region. Recent experimental data (Konrad and Smits, 1998) show that a Mach 3 adiabatic boundary layer matches the Van-Driest law in the logarithmic region. Note that the adiabatic wall temperature increases by 47% in going from $M = 3$ to $M = 4$. Also, the temperatures in the DNS are much higher than those in the experiment because the experiment was conducted with a cold free-stream (total temperature of approximately 265 K). It is uncertain whether there is an edge temperature effect that modifies the scaling of the law of the wall.

Figure 5 plots the temperature contours along planes perpendicular to the flow direction. Since the wall temperature is very high, the bursting events are clearly seen as the hot fluid from the near-wall region mixes into the cold fluid above. We observe the typical mushroom-shaped structures associated with turbulent boundary layers. However, these structures are

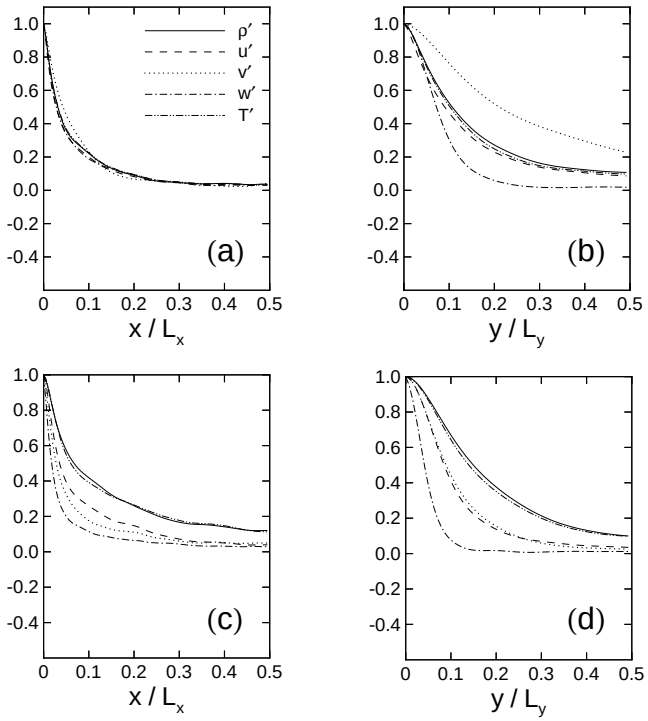

Figure 2. Two-point correlations for the non-reacting simulation, (a)-(b) $z^+ = 110$, and (c)-(d) $z^+ = 4.25$.

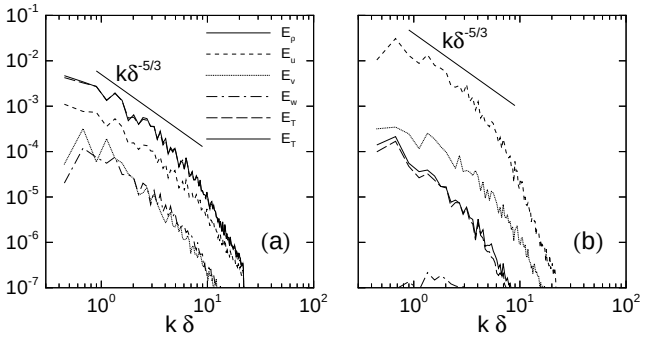

Figure 3. Two-dimensional energy spectra at (a) $z^+ = 110$, and (b) $z^+ = 4.25$, for the non-reacting simulation.

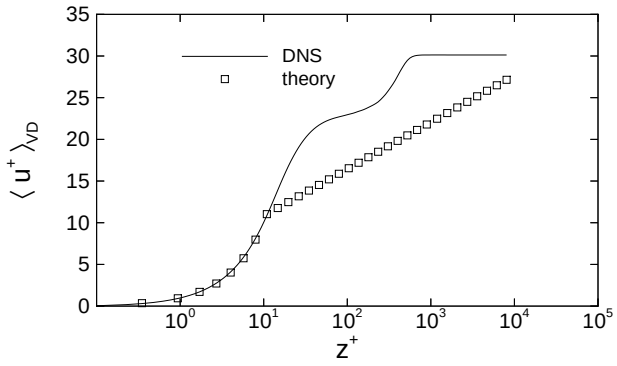

Figure 4. Mean velocity profile scaled on inner variables, and compared to the theoretical $u^+ = z^+$, and Van-Driest empirical $u^+ = 2.44 \log z^+ + 5.2$ scaling laws for non-reacting simulation.

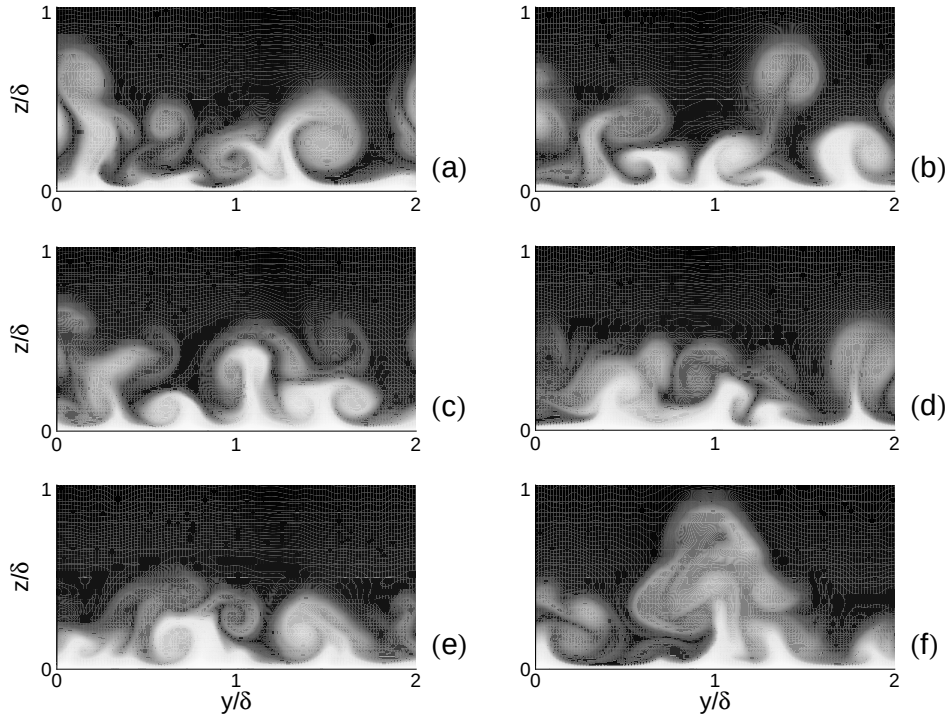

Figure 5. Temperature contours along the spanwise direction for the non-reacting simulation, (a) $x = \delta/8$, (b) $x = \delta/4$, (c) $x = 3\delta/8$, (d) $x = \delta/2$, (e) $x = \delta$, and (f) $x = 3\delta/2$.For a color version visit our web site at *www.arc.umn.edu/ martin/research.html.*

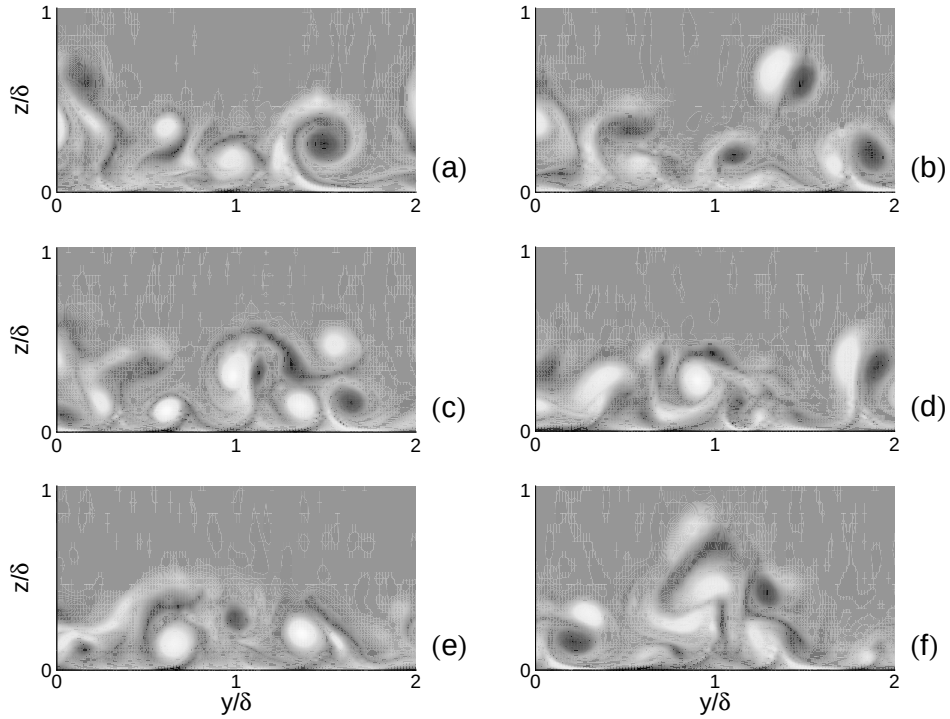

Figure 6. Streamwise vorticity contours along the spanwise direction for the non-reacting simulation. (a) $x = \delta/8$, (b) $x = \delta/4$, (c) $x = 3\delta/8$, (d) $x = \delta/2$, (e) $x = \delta$, and (f) $x = 3\delta/2$.

significantly larger than previously observed in experiments with lower compressibility levels and temperature fields.

Figure 6 plots the streamwise component of vorticity along the spanwise direction. We observe that the eddy structures are composed of counter-rotating vortices that enhance mixing. Although these structures comprise large portions of the boundary layer, it is found that they dissipate in less than 70 wall units in the streamwise direction.

4. Reacting simulations

As a preliminary analysis of the turbulent-chemistry interaction in the boundary layer, the reacting adiabatic simulation is considered. Under the temperature conditions chosen, the reaction $\mathrm{S1} + \mathrm{M} \rightleftharpoons \mathrm{S2} + \mathrm{M}$ is endothermic across the boundary layer. To achieve exothermic reactions, the sign of the heat of formation is changed. In this section, the non-reacting, endothermic, and exothermic simulations for the adiabatic boundary layer are compared.

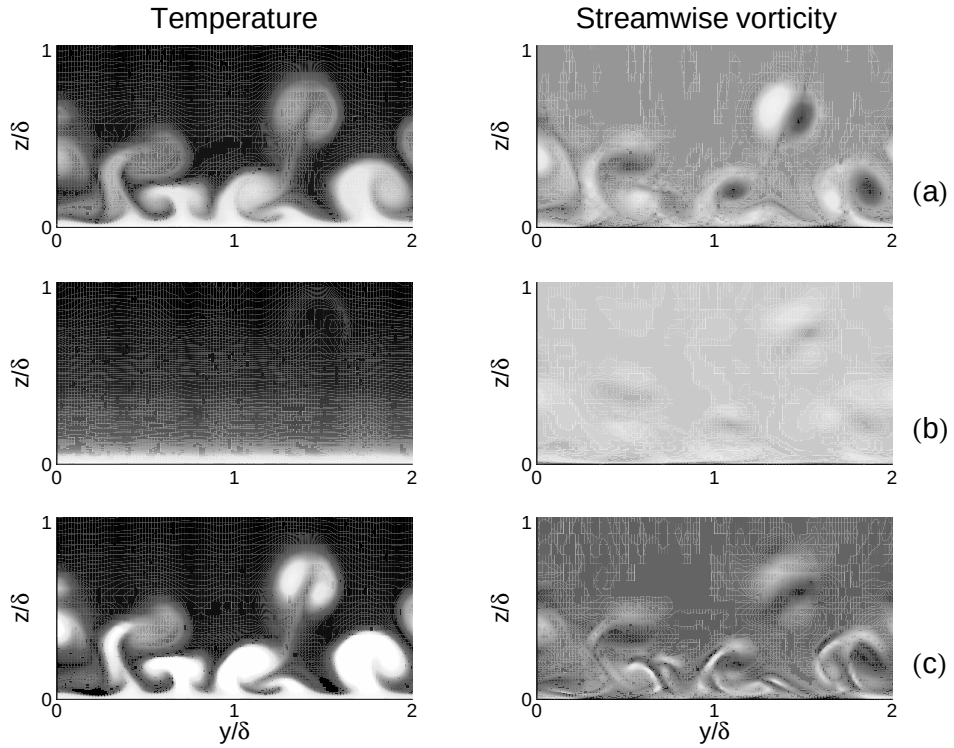

Figure 7. Temperature (left) and streamwise vorticity (right) contours along the spanwise direction for the (a) non-reacting, (b) endothermic, and (c) exothermic simulations, $x = \delta/4$.

Figure 7 plots temperature contours along the spanwise direction. We observe that for the endothermic simulation, the vortical structures are annihilated. Thus, the temperature increases continuously from the boundary layer edge to the wall. In contrast, for the exother-

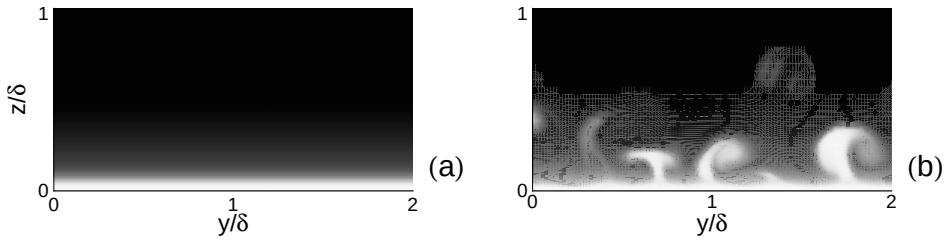

Figure 8. Product mass-fraction contours along the spanwise direction for the (a) endothermic, and (b) exothermic simulations, $x = \delta/4$.

mic simulation, the temperature at the core of the mushroom-shaped structures increases. Thus, the exothermic reactions occur locally, and in regions of the flow where the temperature is highest. Figure 7 also plots the streamwise vorticity along the spanwise direction for the same simulations. For the endothermic simulation, the magnitude of vorticity decreases, and we can hardly see the vortex dipoles. However, for the exothermic simulation, the vorticity magnitude increases at the cores of the vortex pairs. The localized addition of energy causes compressions and expansions that flatten and elongate the cores of the vortex pairs.

Figure 8 plots the product mass-fraction contours for the reacting simulations. For the endothermic simulation, the chemical composition does not differ significantly from the initial condition. In contrast, for the exothermic simulation, the product mass fraction increases in regions where the magnitude of the temperature fluctuations is high.

Figure 9 plots the magnitude of the temperature fluctuations for the three simulations. We observe that the magnitude decreases when the reactions are endothermic. In contrast, when the reaction is exothermic, the magnitude increases up to 110% of the average temperature. Finally, Fig. 10 plots the mass fraction of species S2 normal to the surface. The solid line represents the initial mass fraction. For the endothermic simulation, there is very little activity in the production or destruction of S2. However, there is significant production for the exothermic simulation.

5. Summary

The initialization and resolution requirements for a Mach 4, $Re_\theta = 8200$ boundary layer have been presented. It is found that the domain size and grid resolution are adequate to perform the direct numerical simulations. The preliminary results for an adiabatic boundary layer have been discussed.

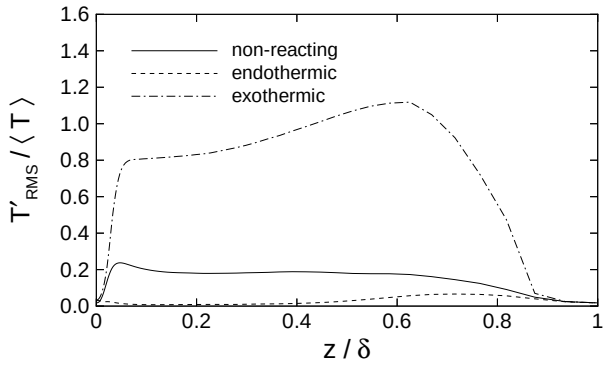

Figure 9. Normalized magnitude of the temperature fluctuations for the non-reacting, endothermic, and exothermic simulations.

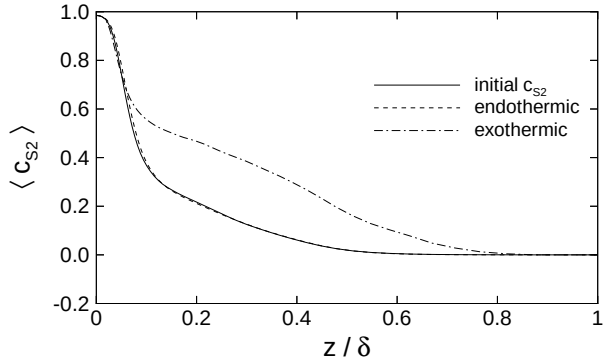

Figure 10. Mass fraction of S2 species for the endothermic and exothermic simulations.

For the non-reacting simulation, it is found that the turbulent mixing of hot and cold fluid substantial. This process generates large mushroom-shaped structures that comprise large portions of the boundary layer. The cores of these structures are composed of counter-rotating vortex pairs. It is found that these structures observed in the spanwise planes dissipate quickly in the streamwise direction. A possible explanation for this is the increase in dissipation due to the presence of shocks. However, a careful shock detection study has not been performed yet. The mean velocity with Van-Driest transformation given by the DNS and the empirical prediction were not in agreement. For the conditions chosen, the adiabatic wall temperature was nearly 18500 K. It is not clear whether the significantly higher adiabatic wall temperature simulation should reproduce the theoretical results, which are predicted for much lower temperature fields. Further

analysis is required to assess whether there is an edge temperature effect that may explain the stronger mixing and modified mean velocity profile that are predicted by the DNS.

For the endothermic reacting simulations, the energy removed by the reaction results in annihilation of the vortical structures in the temperature field and weakening of the vortex dipoles. In contrast, the heat released by the exothermic reaction increases the strength of the vortices. The energy release induces localized expansions and compressions that elongate the cores of the vortex pairs.

As in the case of the reacting isotropic turbulence (Martín and Candler, 1998), it is found that the exothermic reactions increase the magnitude of the temperature fluctuations, while the reaction rate is increased by the turbulent temperature fluctuations. The opposite occurs when the reaction is endothermic.

Acknowledgments

We would like to acknowledge the support from the Air Force Office of Scientific Research Grant number No. AF/F49620-98-1-0035. This work was also sponsored by the Army High Performance Computing Research Center under the auspices of the Department of the Army, Army Research Laboratory cooperative agreement number DAAH04-95-2-0003 / contract number DAAH04-95-C-0008, the content of which does not necessarily reflect the position or the policy of the government, and no official endorsement should be inferred. A portion of the computer time was provided by the University of Minnesota Supercomputing Institute.

References

Candler, G.V., Wright, W.J., and McDonald, J.D. (1994) Data-Parallel Lower-Upper Relaxation method for reacting flows, *AIAA Journal*, **32**, pp. 2380–86.

Johnson, H., Seipp, T., & Candler, G.V. (1998) Numerical study of hypersonic reacting boundary layer transition on cones. *Physics of Fluids,* **10**, pp. 2676–85.

Jones, W.P., and Launder, B.E. (1992) The prediction of laminarization with a two-equation model of turbulence, *International Journal of Heat and Mass Transfer,* **15**, pp. 301–14.

Konrad, W., and Smits, A.J. (1998) Turbulence measurement in a three-dimensional boundary layer in supersonic flow, *Journal of Fluid Mechanics*, **372**, pp. 1–23.

Martín, M.P., and Candler, G.V. (1998) Effect of Chemical reactions on decaying isotropic turbulence. *Physics of Fluids,* **10**, pp. 1715–24.

Martín, M.P., Olejniczak, D.J., Weirs, V.G., and Candler, G.V. (1998) DNS of reacting hypersonic turbulent boundary layers, *AIAA Paper No. 98-2917.*

Morkovin, M.V. (1962) Effects of compressibility on turbulent flows, A.J. (ed) of *Mèchanique de la Turbulence*, pp. 367–80, CNRS.

Olejniczak, D.J., and Candler, G.V. (1997) A Data-Parallel LU relaxation method for DNS of compressible flows, *Proceedings of the First AFOSR International Conference on DNS and LES,* Ruston, LA, Paper No. N-03, Aug. 1997.

Weirs, V.G., and Candler, G.V. (1997) Optimization of weighted ENO schemes for DNS of compressible turbulence, *AIAA Paper No. 97-1940*.